Received 02 September, 2018; | Revised 24 October, 2018; | Accepted 01 December, 2018

DOI: 10.1002/eqe.3147

RESEARCH ARTICLE

Seismic protection of rocking structures with inerters

Rodrigo Thiers-Moggia | Christian Málaga-Chuquitaype

[1]Department of Civil and Environmental Engineering, Imperial College London, London, United Kingdom

Correspondence
Christian Málaga-Chuquitaype
Email: c.malaga@imperial.ac.uk

Present Address
Department of Civil and Environmental Engineering, Imperial College London, Room 322, Skempton Building, London, SW7 2AZ, UK.

Summary

The seismic behaviour of a wide variety of structures can be characterized by the rocking response of rigid blocks. Nevertheless, suitable seismic control strategies are presently limited and consist mostly on preventing rocking motion all together, which may induce undesirable stress concentrations and lead to impractical interventions. In this paper, we investigate the potential advantages of using supplemental rotational inertia to mitigate the effects of earthquakes on rocking structures. The newly proposed strategy employs inerters, which are mechanical devices that develop resisting forces proportional to the relative acceleration between their terminals and can be combined with a clutch to ensure their rotational inertia is only employed to oppose the motion. We demonstrate that the inclusion of the inerter effectively reduces the frequency parameter of the block, resulting in lower rotation seismic demands and enhanced stability due to the well-known size effects of the rocking behaviour. The effects of the inerter and inerter-clutch devices on the response scaling and similarity are also studied. An examination of their overturning fragility functions reveals that inerter-equipped structures experience reduced probabilities of overturning in comparison with un-controlled bodies, while the addition of a clutch further improves their seismic stability. The concept advanced in this paper is particularly attractive for the protection of rocking bodies as it opens the possibility of non-locally modifying the dynamic response of rocking structures without altering their geometry.

KEYWORDS:
Rocking motion, inerter, clutch, pulse-like ground motion, seismic control, dimensional analysis

1 | INTRODUCTION

The dynamic behaviour of a wide range of structural systems, including historical buildings[1,2], post-tensioned structures[3,4,5], bridges[6], walled-structures[7], and unanchored equipment[8,9], can be characterized by the rocking response of a rigid block. After noting the survival of several tall slender structures following severe ground shaking, Housner[10] examined the dynamic behaviour of rigid bodies and developed equations to describe their rocking motion based on an elegant use of momentum conservation through impact. Several researchers have built on Housner's classical model, extending their analyses to rocking frames[11,12] and 3-dimensional rocking structures[13,14]. Although a precise predicition of the full response history of a rocking oscillator under a given ground motion may be impractical[15] due to the strong non-linearities involved (e.g. negative stiffness[16]) and the uncertainties associted with modelling impact pehomena[17,18], Housner's model has been shown capable of predicting the main statistics of the seismic response of rocking structures[19]. In this regard, early studies recognized that rocking motion is highly sensitive to the velocity and acceleration characteristics of the ground motion[20]. Dimitrakopoulos and DeJong[21] studied

the deterministic response of rocking structures to simplified pulse-type excitations and proposed a group of dimentionless-orientationless parameters that define a unique response for slender blocks, and a practically self-similar response for non-slender structures. Several other researchers have proposed the use of intensity measures based on the peak ground velocity (PGV) and peak ground acceleration (PGA)[22,23], while Giouvanidis and Dimitrakopoulos[24] found that an intensity measure which efficiently correlates with the rocking demand is not necessarily efficient for predicting overturning. More specifically, they showed that rocking amplification is sensitive to the duration of the ground motion exceeding the uplifting threshold, whereas the overturning response depends strongly on the velocity and acceleration features of the ground excitation.

In comparison with studies concerning the estimation of rocking response, investigations on control strategies suitable to rocking bodies have been more limited and have mainly concentrated on the protection of museum artefacts and non-structural equipment[25,26]. Early strategies were based on simple measures, such as lowering the centre of mass or anchoring the object to a fixed support[27,28]. While the former approach is not very practical, the latter prevents the rigid-body rocking motion and may therefore induce undesirable deformations that can damage the object. In order to reduce the seismic demands without hindering rocking, a number of researchers have proposed the use of passive and semi-active strategies. De Leo et al.[29] studied the use of a pendulum mass damper hinged at the top of the block, while Ceravolo et al.[26,30] examined semi-active anchorages with variable stiffness and compared different strategies for their implementation. Similarly, Vassiliou and Makris[31] studied the rocking response and stability of rigid blocks standing free on three different types of isolated bases, concluding that seismic isolation is only beneficial for small structures.

An efficient seismic control strategy that has been gaining popularity over the last years involves the use of supplemental rotational inertia. Based on this concept, Arakaki et al.[32] developed a damper formed of a cylindrical mass rotating inside a chamber filled with a viscous fluid. This mechanical arrangement, known as inerter, develops a resisting force that is proportional to the relative acceleration between its terminals. When amplifying mechanisms such as ball-screws[33] or geared wheels[34] are used, high levels of inertial mass can be achieved while keeping the associated gravitational mass at a minimum. Hwang et al.[35] investigated the vibration control effect of a rotational inertia damper combined with a toggle bracing on a single-degree-of-freedom structure. Makris and Kampas[36] studied the case of an elastic frame connected to rack-pinion-flywheel system and demonstrated that inerters are particularly effective in reducing peak displacements for long period structures. Importantly, they noted that this happens at the expense of transferring considerably forces to the support of the flywheels. Their study also explored the use of a clutch to ensure the inerter only resists the structural motion without inducing additional deformations. This arrangement was able to further reduce the structural displacements, whereas mixed results were obtained for the transferred forces. Likewise, several applications of the inerter have been proposed within the context of enhancing the performance of tuned mass dampers[37,38]. All these previous studies have focused on the seismic control of fixed-based structures, where the seismic-induced displacements are governed primarily by the structural stiffness, damping and strength[39,40]. In the case of rocking structures, the dominant motion is rotational and the seismic stability originates mainly from the difficulty of mobilizing its rotational inertia[41]. In this context, the use of supplemental rotational inertia appears as an attractive alternative to improve the seismic performance of rocking structures.

In this paper, we examine the rocking response and stability of rigid blocks equipped with supplemental rotational inertia devices. Besides comparing the response of rocking oscillators equipped with an inerter that can oppose and drive the motion against the response of un-controlled rocking blocks, we also study the effects of adding a pair of clutched inerters designed to only resist the motion. The following section presents original equations that govern the rocking motion of the inerter-rocking system derived by considering a simple discontinuous acceleration-based function for the clutch. Subsequently, we study the effects of the inerter on the self-similar scaling of the response, as well as on associated rocking demands and overturning potential of the blocks under a wide range of trigonometric pulse excitations. Finally, a probabilistic assessment of the seismic performance of rocking blocks is conducted using a set of 202 pulse-like ground motions obtained from the Pacific Earthquake Engineering Research Center (PEER) database. We demonstrate that rocking structures equipped with a single inerter experience smaller rotation and acceleration demands than unprotected ones, and that the incorporation of the clutch further reduces their rotation demands as well as their probability of overturning.

2 | ROCKING STRUCTURES AND SUPPLEMENTAL ROTATIONAL INERTIA

2.1 | Seismic response of rigid rocking blocks

When subjected to a horizontal ground excitation, $\ddot{u}_g$, the rigid block shown in Figure 1 uplifts and starts rocking if the overturning moment exceeds the restoring moment due to its self-weight, this condition can be expressed as:

$$\ddot{u}_g \geq g \tan\alpha \tag{1}$$

where g is the acceleration of gravity and α is the slenderness of the block. Assuming that no sliding or bouncing occurs during impact, the planar rocking motion of the structure can be described by means of Housner's model[10] as:

$$\ddot{\theta} = -p^2 \left(\sin(\alpha\, sgn(\theta) - \theta) + \frac{\ddot{u}_g}{g} \cos(\alpha\, sgn(\theta) - \theta) \right) \tag{2}$$

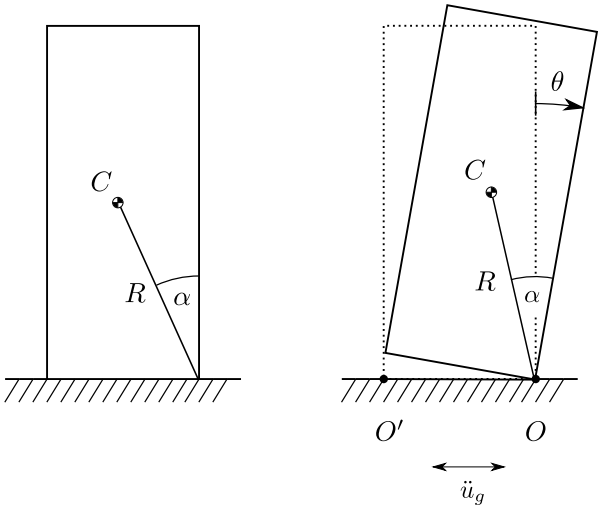

FIGURE 1 Rigid block under a horizontal ground excitation.

Although the free vibration frequency of a rocking block is not constant, its dynamic properties can be characterized by the frequency parameter p, which represents the in-plane pendulum frequency of the same block dangling from its pivot point[42]. For a rectangular block $p = \sqrt{3g/4R}$.

When the angle of rotation θ reverses, the block impacts on the base and loses some of its kinetic energy. Assuming that there is no bouncing, the block then continues rotating smoothly around point O'. Energy losses due to impact are usually considered through a coefficient of restitution that relates the pre-impact angular velocity, $\dot{\theta}_1$, to the post-impact angular velocity, $\dot{\theta}_2$.

$$\dot{\theta}_2 = \eta\, \dot{\theta}_1 \tag{3}$$

By equating the moment of momentum before and after impact, Housner derived an expression for the coefficient of restitution that depends on the geometry and mass of the block. In this paper, we consider η to be an independent parameter of the rocking problem and assume $\eta = 0.85$. A more detailed analysis of the impact problem is beyond the scope of this study (please see El Gawady *et al.*[43] and references therein).

2.2 | Supplemental rotational inertia: the inerter

As stated above, the inerter is a linear mechanical device that develops a resisting force proportional to the relative acceleration between its terminals[34]. Although several types of inerters have been proposed and patented, the general properties of the system

can be studied by considering the particular case of a rack-pynion-flywheel device, like the one shown in Figure 2a. The system consists of two flywheels of radius R_i and mass m_{wi}, free to rotate about axis O_i and connected to a linear rack through a pinion-gear mechanism. Figure 2b shows the free-body diagram of the rotating flywheels.

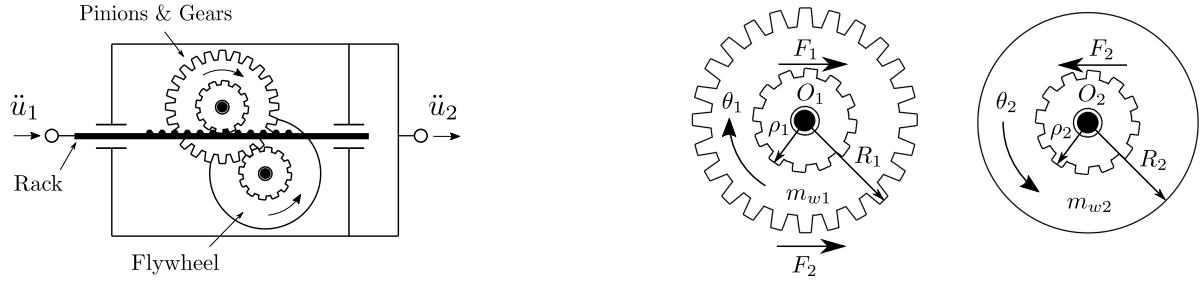

(a) Two-flywheel configuration. **(b)** Free-body diagram of the flywheels.

FIGURE 2 Rack-pynion-flywheel supplemental rotational inertia system.

When a positive relative displacement is imposed ($u_2 > u_1$), the first flywheel is subjected to a clockwise rotation θ_1, while the second flywheel rotates θ_2 anti-clockwise. If there is no slippage between the rack, pinions and gears, the rotations and relative displacement are related through:

$$\theta_1 = \frac{u_2 - u_1}{\rho_1} \quad ; \quad \theta_2 = \frac{(u_2 - u_1)\, R_1}{\rho_1\, \rho_2} \tag{4}$$

Evaluating the rotational equilibrium of the flywheels around pivot points O_1 and O_2 yields:

$$F_1\, \rho_1 = I_{w1}\, \ddot{\theta}_1 + F_2\, R_1 \tag{5}$$

$$F_2\, \rho_2 = I_{w2}\, \ddot{\theta}_2 \tag{6}$$

where $I_{wi} = \frac{1}{2}\, m_{wi}\, R_i^2$ is the moment of inertia of the flywheel around point O_i. Replacing Equation 4 into Equation 5 and combining it with 6 leads to:

$$F_1 = m_r\, (\ddot{u}_2 - \ddot{u}_1) \tag{7}$$

with:

$$m_r = \frac{1}{2}\, \frac{m_{w1}\, R_1^2}{\rho_1^2} + \frac{1}{2}\, \frac{m_{w2}\, R_1^2\, R_2^2}{\rho_1^2\, \rho_2^2} \tag{8}$$

where m_r is the inertance or apparent mass of the inerter. The inertance of the system can be significantly amplified by installing multiple flywheels in series connected through a gearing system. The previous derivation can be extended to a system with n rotating flywheels where the apparent mass of the system is given by[34]:

$$m_r = \frac{1}{2}\, \frac{m_{w1}\, R_1^2}{\rho_1^2} + \frac{1}{2}\, \frac{m_{w2}\, R_1^2\, R_2^2}{\rho_1^2\, \rho_2^2} + \ldots + \frac{1}{2}\, \frac{m_{wn}\, R_1^2\, R_2^2 \ldots R_n^2}{\rho_1^2\, \rho_2^2 \ldots \rho_n^2} \tag{9}$$

Regardless of how small the total mass of the inerter is, any value of inertance can be obtained with the sufficient number and size of flywheels[36]. For instance, for a two-flywheel system of radius ratio $R_i/\rho_i = 10$, only one ten thousandth of the structure's mass, m, would be required to obtain a mass ratio, m_r/m, of 0.5.

Makris and Kampas[36] recognized that the rotating flywheels store energy that is then transferred back to the primary structure. To overcome this issue, they proposed the use of two parallel rotational inertia systems equipped with clutches to ensure the rotational inertia only opposes the motion without inducing additional deformations. A dissipative mechanism is needed to

decelerate the flywheel once it disengages. Assuming an acceleration-based clutch, the sequential engagement of the two parallel inerters can be expressed mathematically as:

$$F_1(t) = \begin{cases} m_r\, \ddot{u}, & \left[\frac{\ddot{u}}{\dot{u}}\right] > 0 \\ 0, & \left[\frac{\ddot{u}}{\dot{u}}\right] < 0 \end{cases} \tag{10}$$

2.3 | Rocking block - inerter systems

The overall rational behind our proposal is that the vibration absorbing capabilities of supplemental rotational inertia devices can be applied to the seismic protection of rocking structures. To this end, Figure 3 shows some possible configurations of the proposed block-inerter system. In the case of single rocking structures (such as storage tanks and post-tensioned columns and walls) a pair of vertical inerters can be attached near their base and connected to a rigid foundation (Figure 3a). In this way, the inerters are sequentially activated by the vertical acceleration at the connected nodes following rocking motion. This configuration will be more effective for stocky blocks, since the vertical acceleration in slender structures will be small. In the case of slender blocks, a horizontal inerter can be used as presented in Figure 3b. In this arrangement a horizontal support will be required to attach the inerter to the structure. This can be useful when protecting electrical equipment or non structural elements that can be tied to a stiff wall or support. Alternatively, a variety of pulley systems can be used to transfer and amplify the acceleration from any tying point within the rocking structure while carrying the forces to a more practical inerter location (as in Figure 3c). This is particularly attractive for the protection of rocking bodies as it opens the possibility of non-locally modifying the dynamic response of rocking structures without altering their geometry.

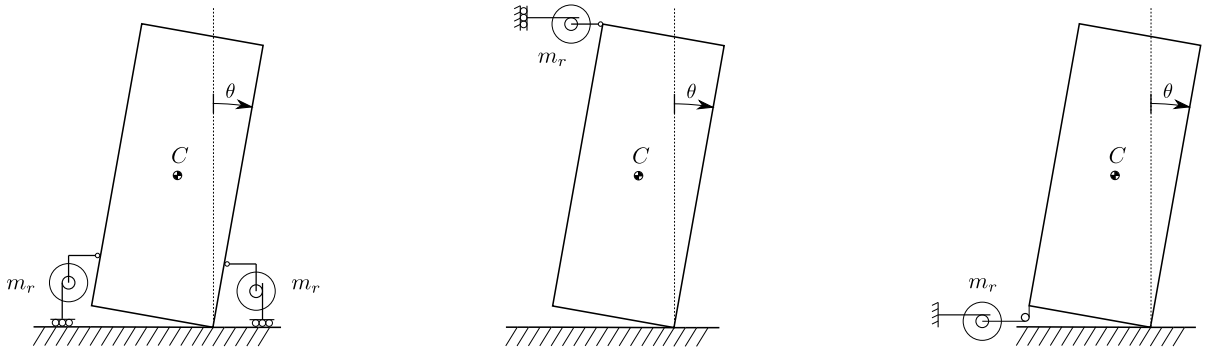

(a) Vertical pair of inerters. **(b)** Horizontal inerter. **(c)** Pulley-inerter system.

FIGURE 3 Examples of rigid block-inerter configurations.

The general dynamic characteristics of the systems depicted in Figure 3 can be studied with reference to the rocking block shown in Figure 4, where a horizontal inerter of apparent mass, m_r, connected to the center of mass is considered for clarity. The rigid block is characterized by its mass, m, and the location of the center of mass, C, defined by the slenderness α and the size parameter R. The block is free to rotate about points O and O' and it is assumed that the coefficient of friction is large enough to prevent sliding between the block and the base. The rotation of the block is measured by the angle θ.

Rocking motion initiates when the overturning moment due to the ground excitation exceeds the restoring moment exerted by the self-weight (Equation 1). Until this instant the resisting force in the inerter is zero, since there is no relative acceleration between its terminals. Once the block uplifts, the tangential relative acceleration at point C is $R\,\ddot{\theta}$. The horizontal linear acceleration depends on the magnitude of the rotation and can be expressed as (Figure 4):

$$\ddot{u} = R\,\ddot{\theta}\cos(\alpha\, sgn(\theta) - \theta) \tag{11}$$

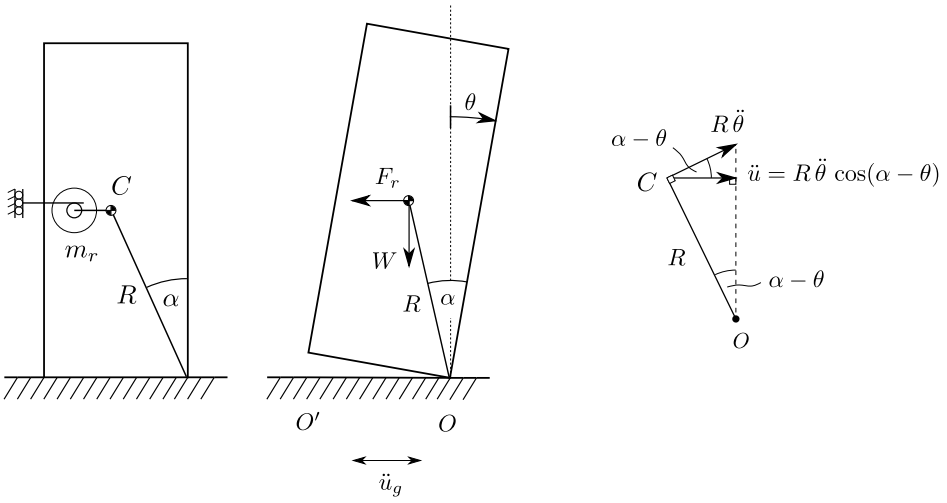

FIGURE 4 Block-inerter system under a horizontal ground excitation.

Therefore, the resisting force in the inerter is:

$$F_r = m_r\, R\,\ddot{\theta}\, cos(\alpha\, sgn(\theta) - \theta) \tag{12}$$

Evaluating the rotational equilibrium around the rocking pivot point gives:

$$\left(I_0 + m_r R^2 \cos^2(\alpha\, sgn(\theta) - \theta)\right)\ddot{\theta} \;+\; mgR\, \sin(\alpha\, sgn(\theta) - \theta) = -m\ddot{u}_g R\, \cos(\alpha\, sgn(\theta) - \theta) \tag{13}$$

where I_0 is the moment of inertia about the centres of rotation O and O'. For rectangular blocks $I_0 = (4/3)mR^2$, and

$$\left(\frac{4R}{3} + \sigma R \cos^2(\alpha sgn(\theta) - \theta)\right)\ddot{\theta} = -g\, \sin((\alpha sgn(\theta) - \theta)) - \ddot{u}_g \cos(\alpha sgn(\theta) - \theta) \tag{14}$$

where $\sigma = m_r/m$ is the apparent mass ratio. Equation 14 can be rearranged to obtain an expression similar to Equation 2:

$$\ddot{\theta} = -p_\sigma^2 \left(\, \sin((\alpha sgn(\theta) - \theta)) + \frac{\ddot{u}_g}{g} \cos(\alpha sgn(\theta) - \theta)\right) \tag{15}$$

with

$$p_\sigma = \sqrt{\frac{3\,g}{R\left(4 + 3\,\sigma \cos^2(\alpha sgn(\theta) - \theta)\right)}} \tag{16}$$

Equation 15 shows that the inclusion of the inerter has an effect equivalent to reducing the frequency parameter, p, of the block. This effect depends on the magnitude of the rotation θ, reaching a maximum when $\theta = \alpha$ and becoming less significant for higher rotations. In general, the reduction of the frequency parameter should result in lower seismic demands due to the size effect of rocking behaviour[10]. This principle dictates that among two blocks of the same slenderness α, the one with the lower frequency parameter, p (larger in size), is more stable and therefore has lower levels of structural demands. It is important to note that for a given rectangular block, the frequency parameter, p, depends only on the size, R, and therefore cannot be modified without altering its geometry. Consequently, the use of supplemental rotational inertia devices configures a practical alternative to modify the dynamic response and reduce seismic demands in rocking structures.

Equation 15 can be linearized if slender blocks are considered (small α), such that:

$$\ddot{\theta} = -p_\sigma^2 \left(\alpha sgn(\theta) - \theta + \frac{\ddot{u}_g}{g}\right) \tag{17}$$

with

$$p_\sigma = \sqrt{\frac{3\,g}{R\left(4 + 3\,\sigma\right)}} \tag{18}$$

Importantly, the clutched-pair-of-inerters proposed by Makris and Kampas[44] can be easily incorporated into the above mathematical formulation. To this end, in order to represent an arrangement that can only resist the rocking motion,, the effects of the apparent mass of the inerter are re-evaluated after each integration step according to Equation 10. Figure 5 compares the response of a slender block equipped with a single inerter (left) and a pair of clutched-inerters (right). The system has a mass ratio $\sigma = 0.5$ and is subjected to a sine pulse ground acceleration of $a_g/g\alpha = 1.5$ and $\omega_g/p = 4$, where a_g and ω_g are the ground acceleration amplitude and frequency, respectively. The sequential engagement and disengagement of the clutched-inerters during the rocking motion can be clearly appreciated in the transferred force response (bottom right panel in Figure 5).

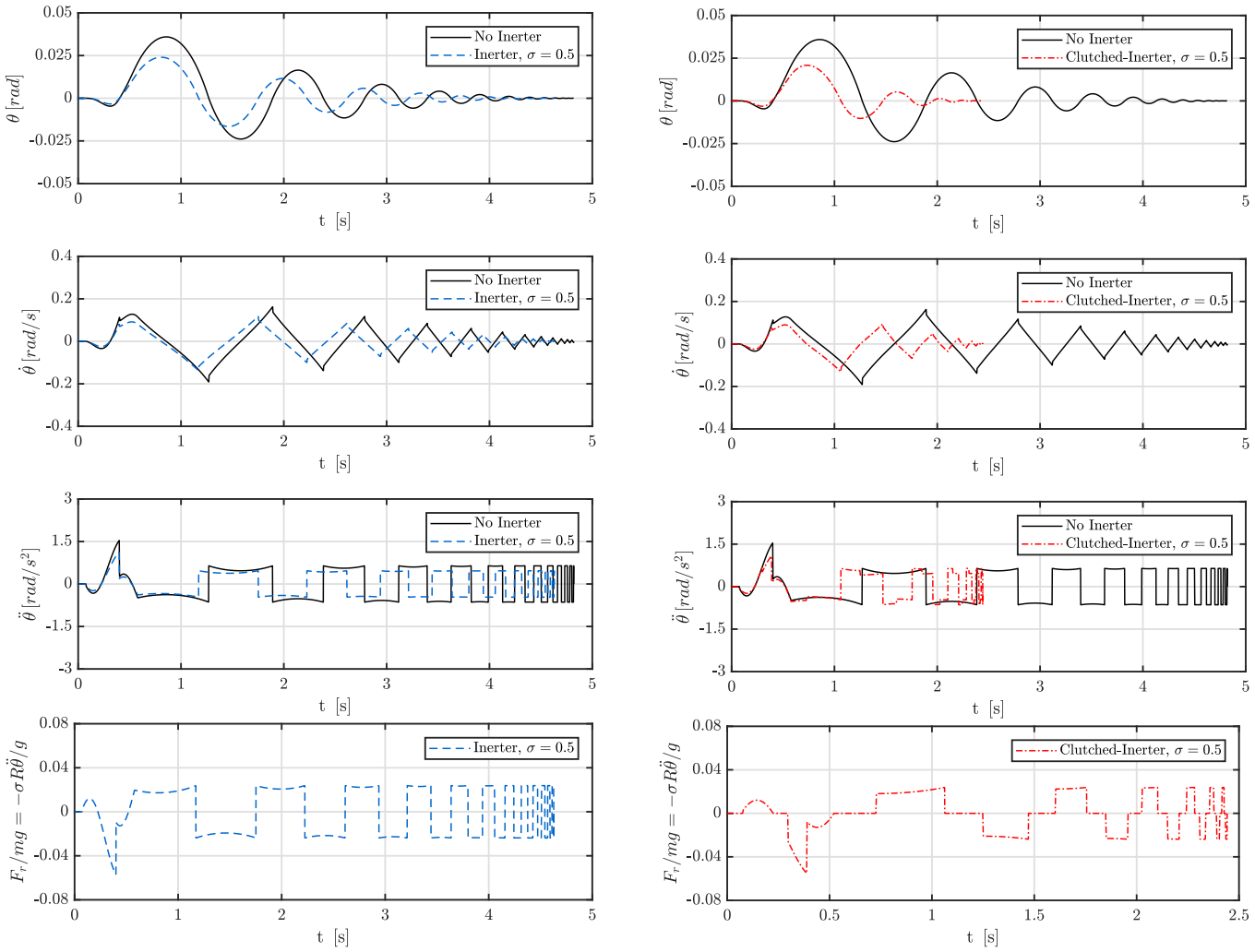

(a) Single Inerter **(b)** Clutched pair of inerters

FIGURE 5 Response of a slender-block-inerter system to a sine pulse ground acceleration

The results plotted in Figure 5 show a significant increase in the energy dissipated by the clutched-inerter configuration, which is reflected in a fastest decrease of the rocking amplitude. This observation may be explained by the assumption underlying Equation 10 by which the energy stored in the idle rotating flywheel is completely dissipated before it re-engages. A more detailed analysis of the rocking demands for a wider range of pulse excitations is conducted in the following sections.

3 | SELF-SIMILAR RESPONSE OF ROCKING BLOCK-INERTER SYSTEMS

The response of a rigid block to an analytical pulse ground motion of acceleration amplitude a_g and dominant frequency ω_g, is a function of 5 variables

$$\theta_{max} = f\left(\alpha\,,\, p\,,\, \frac{a_p}{g}\,,\, \omega_g\,,\, \eta\right) \tag{19}$$

Applying Vaschy-Buckingham's Π-theorem[45,46], the number of independent parameters required to define a unique response can be reduced to 4:

$$\theta_{max} = f\left(\frac{\omega_g}{p}\,,\, \frac{a_g}{g}\,,\, \alpha\,,\, \eta\right) \tag{20}$$

Based on dimentionless and orientationless analysis, Dimitrakopoulos and DeJong[21] showed that the response of slender blocks can be described by 3 dimentionless and orientationless terms:

$$\frac{\theta_{max} g}{a_g} = \phi\left(\frac{\omega_g}{p}\,,\, \frac{g\tan\alpha}{a_g}\,,\, \eta\right) \tag{21}$$

When stocky blocks are considered, α cannot be incorporated entirely into the other parameters and appears as an isolated argument, $\cos(\alpha)$. However, for small rotation angles the influence of α is relatively small and it is convenient to eliminate $\cos(\alpha)$ as an independent group[21] such that:

$$\frac{\theta_{max}\, g}{a_g\, \cos\alpha} \simeq \phi\left(\frac{\omega_g}{p}\,,\, \frac{g\,\tan\alpha}{a_g}\,,\, \eta\right) \tag{22}$$

It can be appreciated from Equation 15 that the inclusion of the inerter only modifies the frequency parameter, p, and as such it should not affect the validity of Equation 21. However, in the case of clutched systems, the inclusion of the inerter-clutch device adds an additional source of non-linearity to the equation of motion, and therefore its self-similar response must be verified. To this end, Figure 6 compares the response of two blocks of dimensionless-orientationless parameters $g\alpha/a_g = 0.57$ and $\eta = 0.85$, connected to a single inerter and to a pair of clutched-inerters, when subjected to a single sine pulse of frequency $w_g/p = 4$. The inerter device is described in terms of the mass ratio $\sigma = m_r/m$, which is a dimensionless-orientationless quantity, and can be treated as an independent parameter such that:

$$\frac{\theta_{max} g}{a_g} = \phi\left(\frac{\omega_g}{p}\,,\, \frac{g\tan\alpha}{a_g}\,,\, \eta\,,\, \sigma\right) \tag{23}$$

It is evident from Figure 6b that, when presented in terms of the proposed parameters, the responses collapse into a single master curve, showing that the inclusion of inerters or clutched-inerters preserves the self-similarity in the response of slender blocks. In the case of non-slender blocks, the effects of the inerter depend on the magnitude of the rotation θ (Equation 15). Therefore, it is expected that the practically self-similar formulation developed by Dimitrakopoulos and DeJong (Equation 22) will not be directly applicable to stocky rocking block-inerter systems. In order to examine this, Figure 7 compares the response of two rocking blocks of equivalent dimensionless-orientationless parameters connected to: i) a single inerter, and ii) a pair of clutched-inerters. The rocking response of these blocks is calculated by solving the full non-linear equation of motion (Equation 15). The left side of Figure 7b shows that the response of the single inerter case remains practically self-similar, as the plots virtually collapse to a single curve. However, the incorporation of the clutch modifies this behaviour and the response becomes non or less self-similar (Figure 7b, right). This is an important finding that affects more the later stage of the response, as can be observed from Figure 7.

4 | OVERTURNING UNDER SINGLE PULSE EXCITATIONS

The rocking response of a rigid block can result in one of two outcomes: i) safe rocking, where the block survives the ground motion and the energy is dissipated through successive impacts at the base until the motion stops; and ii) overturning, where the equation of motion (Equation 15) leads to an arbitrarily large rotation value ($|\theta_{max}|/\alpha \to \infty$) and the block topples. Overturning

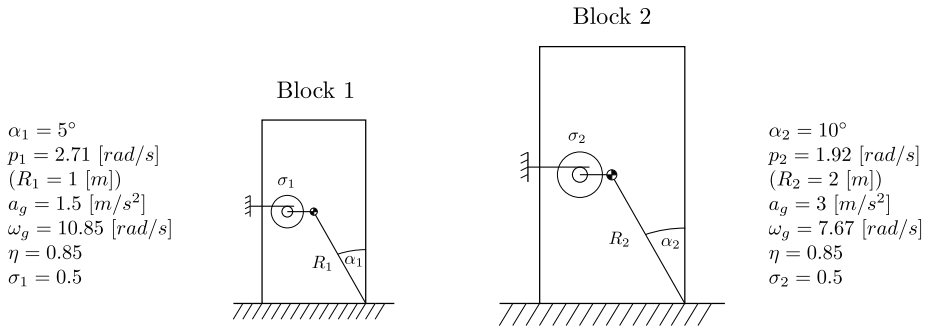

(a) Slender block-inerter systems.

$$\frac{\omega_g}{p} = 4; \qquad \frac{g\alpha}{a_g} = 0.57; \qquad \eta = 0.85; \qquad \sigma = 0.5;$$

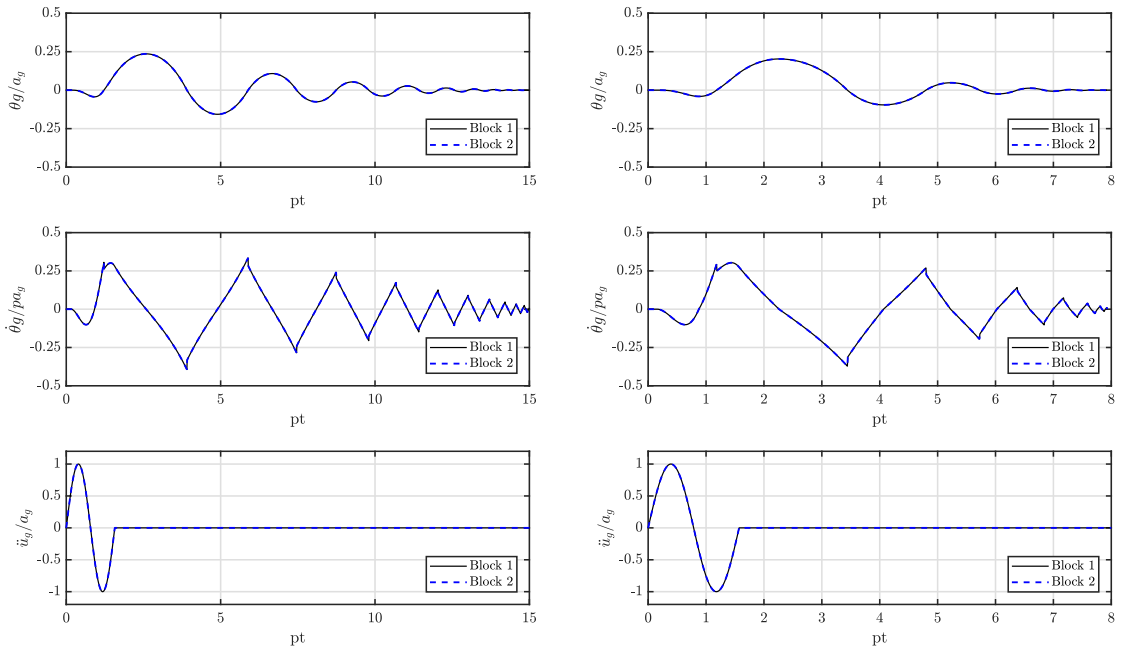

(b) Response of blocks 1 and 2 presented in terms of dimensionless-orientionless parameters.

FIGURE 6 Self-similar response of slender block-inerter systems (small-angle approximation: Equation 17).

is usually studied by means of overturning plots like the ones presented in Figure 8. These plots show the regions in the frequency-amplitude acceleration space that result in safe rocking or overturning of the block. The area above the upper curves in the graphs of Figure 8a represent overturning withouth impact (Region 1), whereas the areas enclosed by the lower curves correspond to overturning taking place after impact at the base[47] (Region 2). The remaining regions of the plot are associated with safe rocking (Region 3).

In this section, we study the effects of incorporating the inerter on the oveturning behaviour of rocking blocks by considering sinusoidal and cosinusoidal acceleration pulses. Figure 8 shows the overturning plots obtained for slender ($\alpha < 10°$) and non-slender blocks ($\alpha = 20°$) equipped with a single inerter and a pair of clutched inerters. It can be appreciated that, in general, the inclusion of the inerter reduces the areas of overturning (Regions 1 and 2), and translates them to the lower frequency region. This frequency shift, which is otherwise beneficial, is particulary relevant for the case of overturning after impact (Region 2), as certain blocks that would rock safely without the inerter, may overturn when the protective device is incorporated. Similar trends are observed for the non-slender block (Figure 8b). The effect of the inerter system on the overturning response is considerably

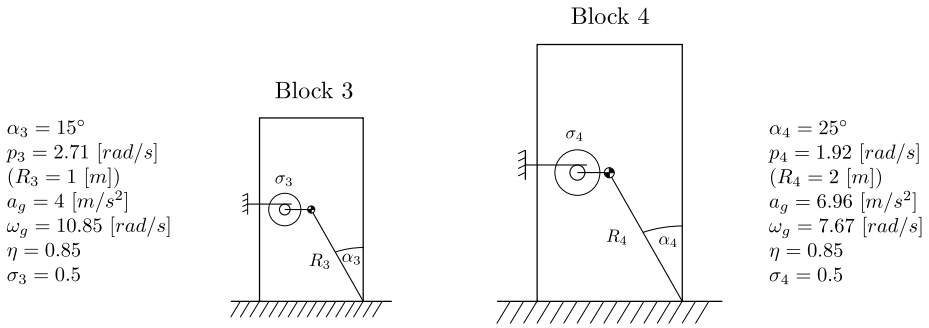

(a) Non-slender block-inerter systems.

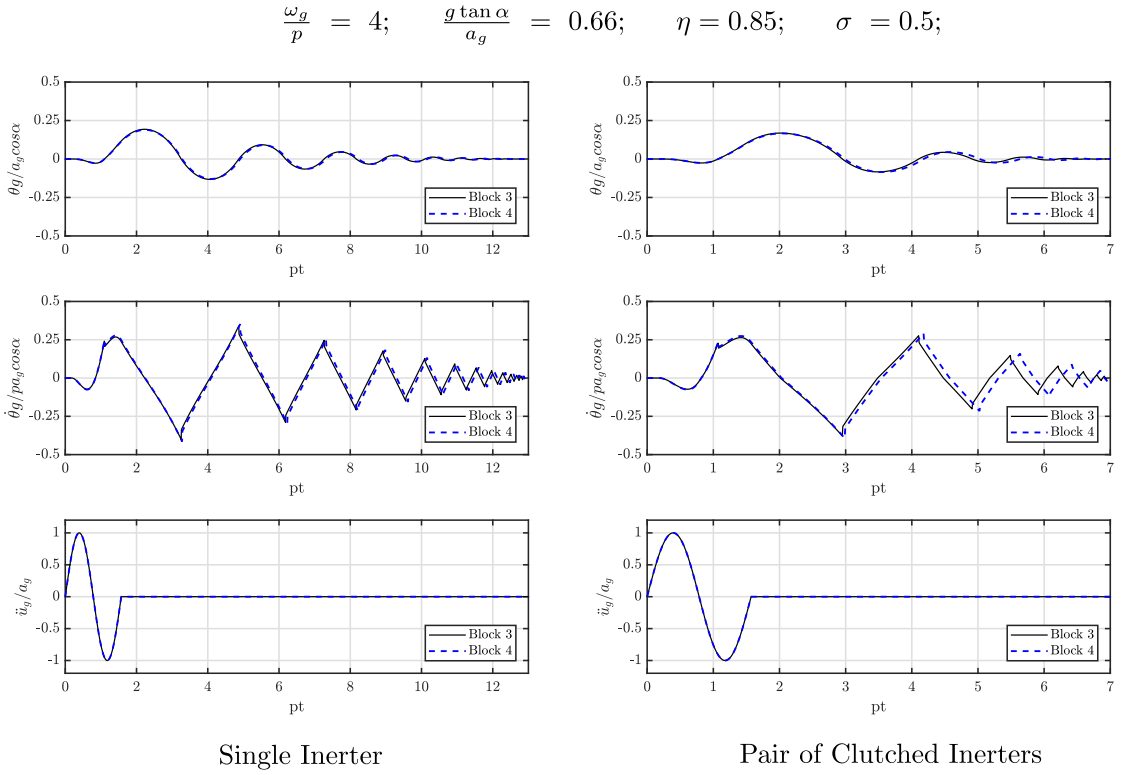

(b) Response of blocks 3 and 4 presented in terms of dimensionless-orientionless parameters.

FIGURE 7 Self-similar response of non-slender block-inerter systems (Equation 15).

less significant for smaller objects ($\omega/p < 2$). Therefore, the use of a higher mass ratio, σ, will be necessary to further improve the stability of such blocks under single pulse excitations.

It is worth noting that overturning without impact can involve motion reversals, especially when clutched inerters are employed, leading to the difference in the overturning plots observed in Figure 8. This can be further examined with reference to Figure 9, where the response of a slender block with no, single, and a pair of clutched inerters is depicted. It can be seen from this figure that the response of the blocks equipped with a single inerter and a pair of clutched inerters are identical until the condition for disengagement is attained (Equation 10), leading to the avoidance of overturning by the twin clutched-inerter configuration.

The incorporation of the clutch shows different results for cosine and sine acceleration pulses. In the first case, a slight reduction in the areas of overturning is observed, with a small further shift to the region of lower frequencies in comparison with the single inerter configuration. This translation is also observed for the sinusoidal pulses. However, in the case of sinusoidal pulses the area of overturning after impact (Region 2) is significantly extended for both slender and stocky blocks. This is an important finding and suggests that although the inerter improves the general overturning resistance of the block, the incorporation of a

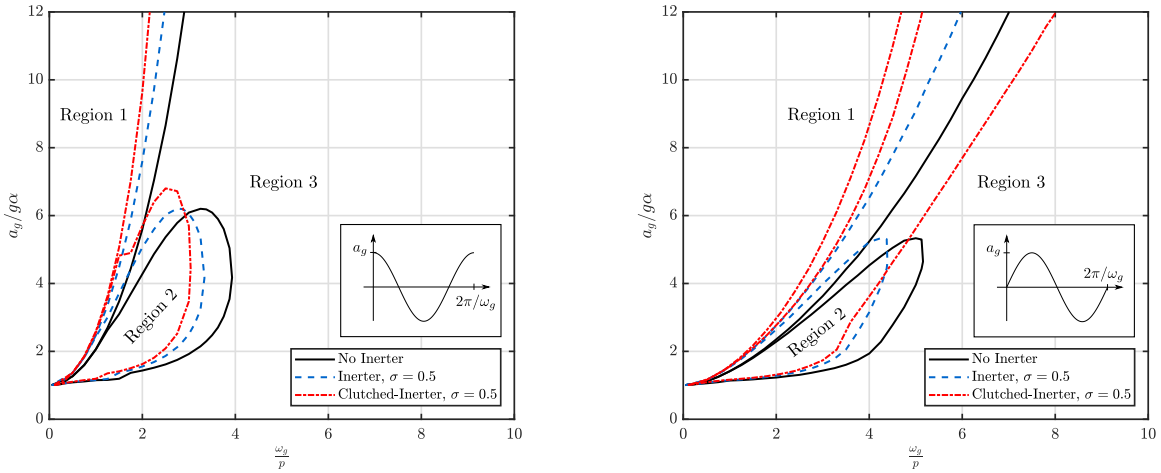

(a) Slender-block-inerter system.

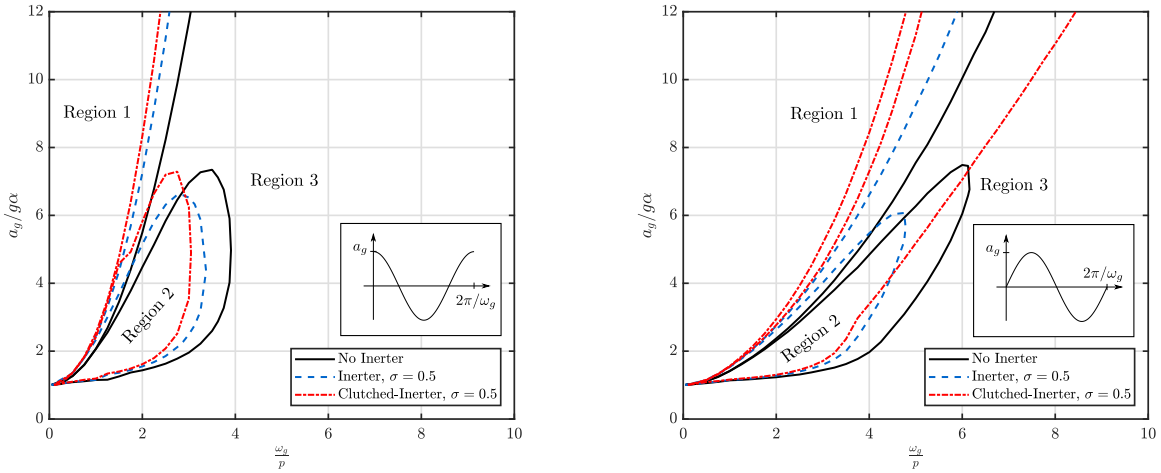

(b) Non-slender-block-inerter system ($\alpha = 20°$).

FIGURE 8 Overturning plots of a rocking-block-inerter systems subjected to trigonometric pulses.

clutch may have a detrimental effect on the rocking response in some cases, especially in relation to overturning after impact. To further examine these effects; Figure 10 compares the rotations of slender blocks with no, single and a pair of clutched inerters under a sine pulse of $\omega/p = 6$ and $a_g/g\alpha = 7.7$. It can be appreciated from this figure that a shift in the impact time is induced by the change in the frequency parameter brought about by the inerter. In the case of the unprotected and single inerter structures, impact takes place close to the end of the sinusoidal excitation meaning that the second half of the pulse, after reversal of acceleration, can effectively help to restrain the motion of these blocks. The introduction of the clutch, however, leads to impact occurring closer to the instant of acceleration reversal, causing most of the second half of the ground motion to exacerbate the rotation after impact.

5 | ROCKING DEMANDS UNDER SINGLE PULSE EXCITATIONS

Even if the block survives the ground motion (no overturning), high rotations and angular accelerations associated with the rocking motion can cause significant damage to the structure and its contents. Our analyses under single pulse excitations (Figure 5), have suggested that the use of supplemental rotational inertia can help to reduce seismic demands and improve the dynamic response of rocking structures. In this section, we offer a more complete analysis considering a wider range of trigonometric

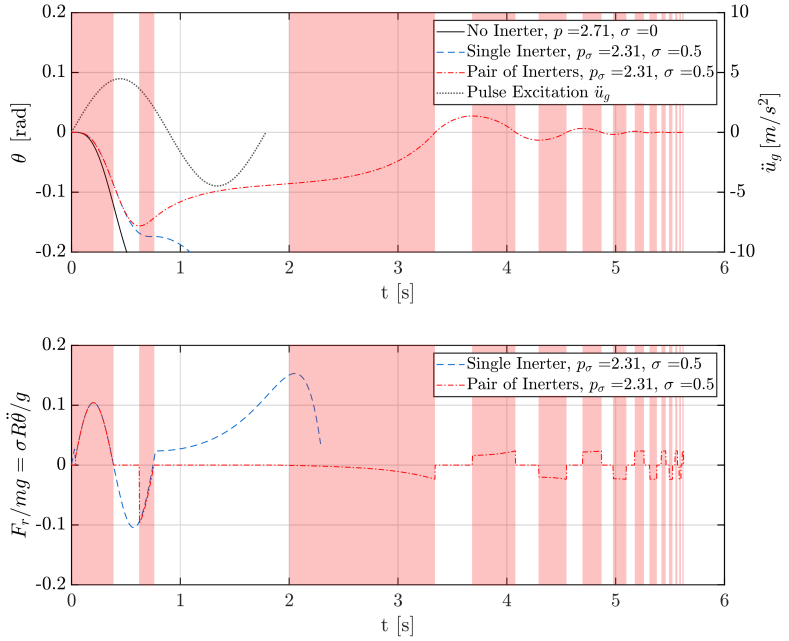

FIGURE 9 Response history of slender blocks to a sine pulse of $\omega/p = 3$,$a_g/g\alpha = 5.22$. The shaded areas show clutch engagement.

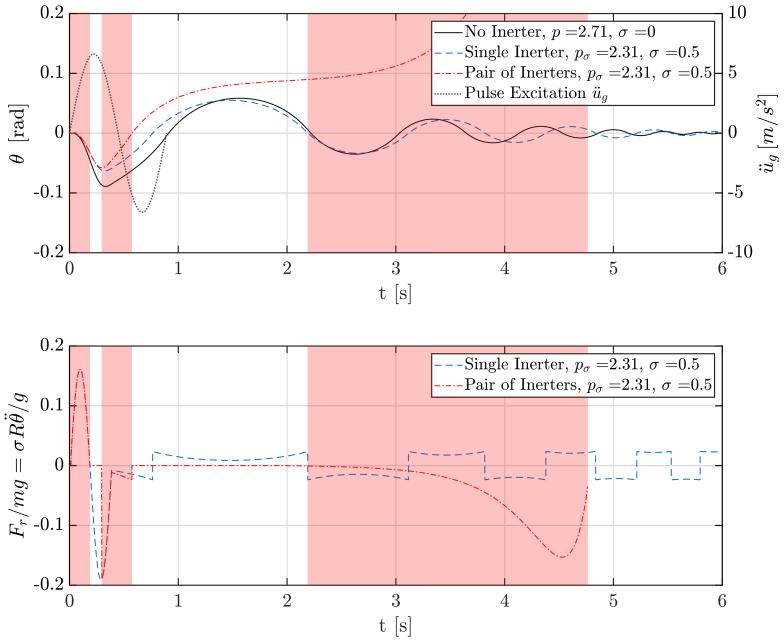

FIGURE 10 Response history of slender blocks to a sine pulse of $\omega/p = 6$,$a_g/g\alpha = 7.7$. The shaded areas show clutch engagement.

pulse excitations. The response parameters are presented in terms of rocking spectra, which consist of contour plots of the normalized response variable in the frequency ratio (ω_p/p) and acceleration amplitude ($a_g/g \tan\alpha$) plane, for a block of a given slenderness α. Accordingly, Figures 11 and 12 compare the rotation and acceleration demands for a rigid block of slenderness $\alpha = 20°$ subjected to cosinusoidal and sinusoidal pulses, respectively, of dominant frequency ω_g and acceleration amplitude a_g.

Results are offered for three different configurations: i) no inerter, ii) single inerter ($\sigma = 0.5$), and iii) pair of clutched inerters ($\sigma = 0.5$).

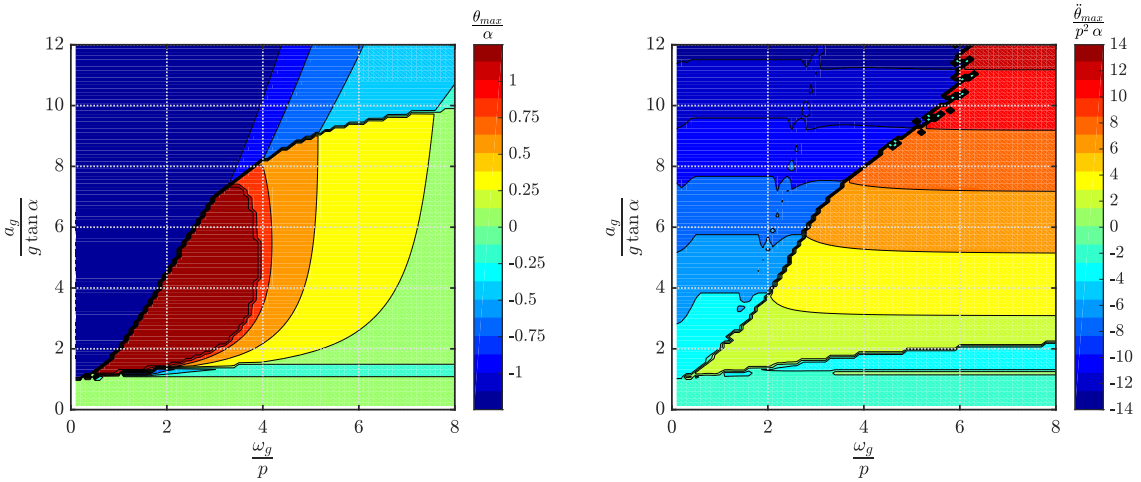

(a) Single rigid block (no inerter).

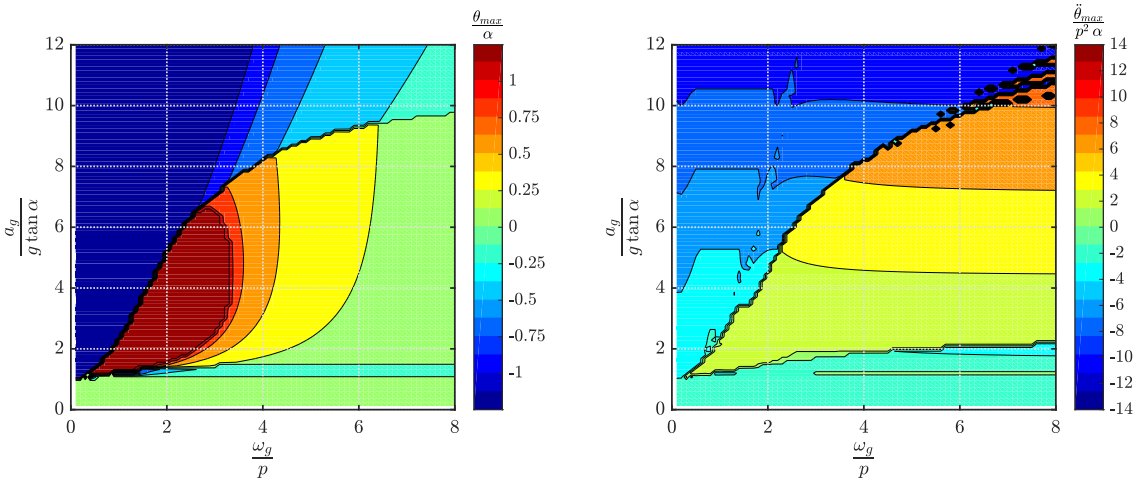

(b) Rigid block connected to a single inerter ($\sigma = 0.5$).

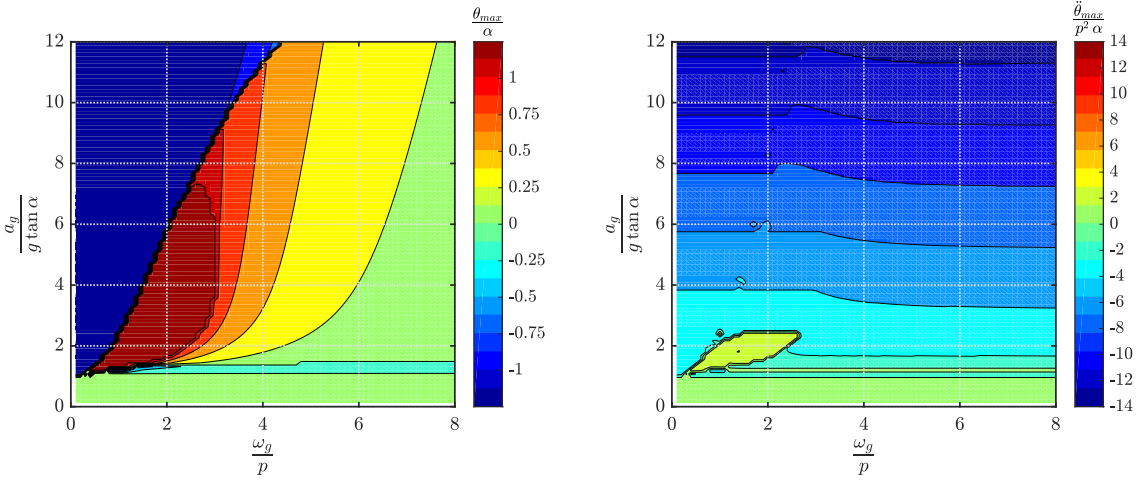

(c) Rigid block connected to a pair of clutched inerters ($\sigma = 0.5$).

FIGURE 11 Rocking spectra for a non-slender block ($\alpha = 20°$) subjected to cosine pulse excitations.

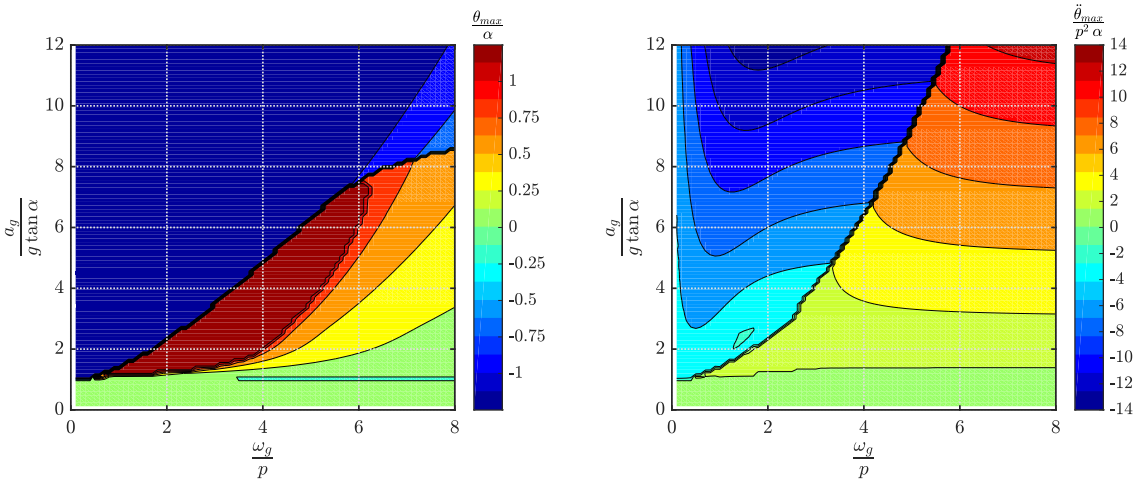

(a) Single rigid block (no inerter).

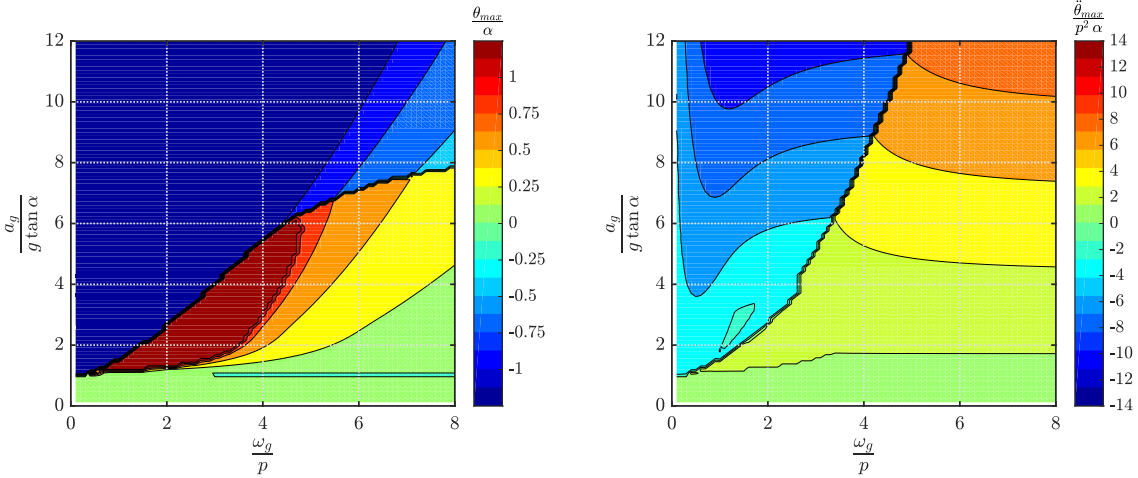

(b) Rigid block connected to a single inerter ($\sigma = 0.5$).

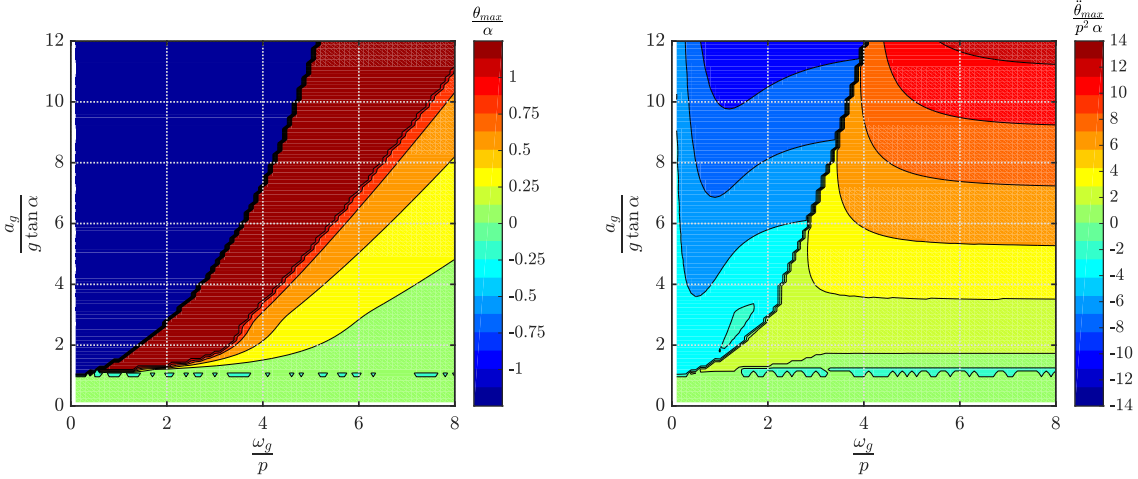

(c) Rigid block connected to a pair of clutched inerters ($\sigma = 0.5$).

FIGURE 12 Rocking spectra for a non-slender block ($\alpha = 20°$) subjected to sine pulse excitations.

The rocking spectra presented in Figures 11 and 12 reveal a considerable reduction in the rotation and acceleration demands for the single inerter case (Figures 11b and 12b). Moreover, the reduction in angular accelerations is more significant for larger

pulse acceleration amplitudes. On the other hand, blocks connected to a pair of clutched inerters (Figures 11c and 12c) exhibit a different behaviour depending on the type of excitation and the magnitude of acceleration amplitude, a_g.

The trends identified above can be better appreciated if a single acceleration amplitude is considered, and the response variables are presented only in terms of the frequency ratio ω_p/p. To this end, Figure 13 compares the response of the same block ($\alpha = 20°$) subjected to cosine and sine pulses of dominant frequency ω_g and acceleration amplitudes $a_g/g\tan\alpha = 2$ and $a_g/g\tan\alpha = 8$ for the three configurations under study.

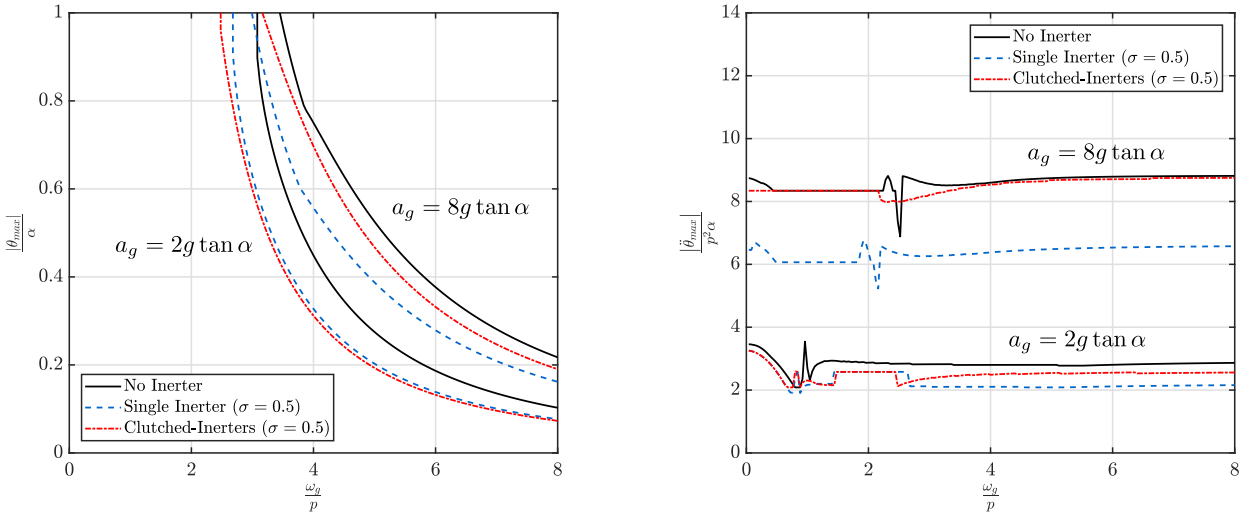

(a) Cosine pulse excitations.

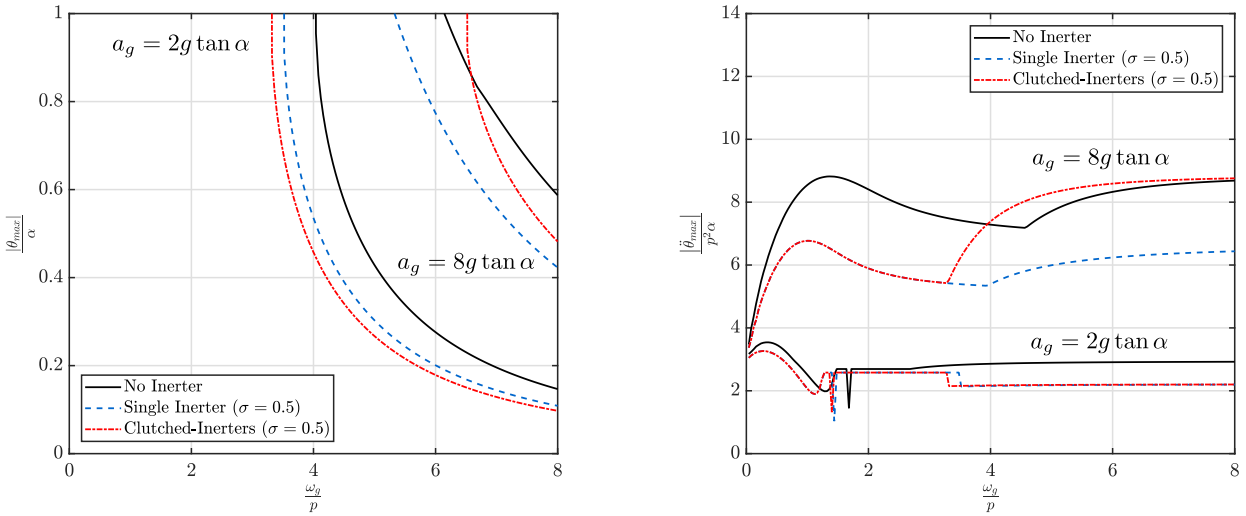

(b) Sine pulse excitations.

FIGURE 13 Rotation and angular acceleration spectra for a non-slender block ($\alpha = 20°$) subjected to trigonometric pulse excitations of $a_g/g\tan\alpha = 2$ and $a_g/g\tan\alpha = 8$.

It can be seen from Figure 13 that under cosine pulse ground motions of small acceleration amplitudes ($a_g/g\tan\alpha \leqslant 2$), the incorporation of the clutch brings minor additional benefits over rotation demands in comparison with the single inerter case. Instead, it increases accelerations for frequency ratios higher than 2 (Figure 13a). For larger accelerations ($a_g/g\tan\alpha \geqslant 8$), the clutch is clearly detrimental, offsetting the reduction brought about by the inerter on the rotations, and practically cancelling it

on angular accelerations. A similar behaviour is observed in the rotation demands for the blocks subjected to sinusoidal pulse excitations. A minor additional reduction can be observed for small amplitude pulses, whereas higher rotation demands are obtained for larger acceleration excitations. The detrimental effects of the clutch on the overturning response are also evident in this region, as the proportion of blocks (frequency ratios) that survive the ground motion is smaller than for the no inerter case. In terms of angular accelerations, the blocks equipped with the pair of clutched inerters show practically the same maximum response than the blocks connected to a single inerter for small acceleration amplitudes ($a_g/g \tan\alpha \leqslant 2$). Moreover, when higher ground motion accelerations are considered ($a_g/g \tan\alpha \geqslant 8$), the addition of the clutch considerably increases acceleration demands, even surpassing the no inerter case. The region where both cases (single inerter and clutched-inerters) overlap corresponds to the area of overturning without impact. In these cases there is no inversion of the direction of motion, and therefore the clutch has no effect on the response. Equivalent analyses were conducted for slender rocking blocks and similar results were obtained.

6 | RESPONSE UNDER REAL PULSE-LIKE GROUND MOTIONS

Previous sections have examined the fundamental dynamic behaviour of rocking blocks equipped with inerter devices subjecting them to single trigonometric pulse excitations. However, recorded near-field ground motions contain, besides coherent long-period pulses, some high frequency spikes and fluctuations that can increase the seismic demands on rocking structures. In this section, we assess the effectiveness of the inerter for the protection of rocking structures employing a set of 202 real pulse-like ground motion records obtained from the Pacific Earthquake Engineering Research Center (PEER) database. Records from 21 earthquakes with magnitudes M_w ranging from 5.4 to 7.9 are considered. Table 1 summarizes the catalogue of earthquakes used in the analyses.

TABLE 1 Ground motion database used in the analyses

Earthquake name	Year	Magnitude M_w	Mechanism	Number of Records
San Fernando	1971	6.61	Reverse	1
Tabas Iran	1978	7.35	Reverse	1
Coyote Lake	1979	5.74	Strike Slip	4
Imperial Valley-06	1979	6.53	Strike Slip	12
Irpinia Italy-01	1980	6.9	Normal	2
Westmorland	1981	5.9	Strike Slip	1
Morgan Hill	1984	6.19	Strike Slip	2
Kalamata Greece-02	1986	5.4	Normal	1
San Salvador	1986	5.8	Strike Slip	2
Superstition Hills-02	1987	6.54	Strike Slip	2
Loma Prieta	1989	6.93	Reverse Oblique	6
Cape Mendocino	1992	7.01	Reverse	1
Landers	1992	7.28	Strike Slip	3
Northridge-01	1994	6.69	Reverse	14
Kobe	1995	6.9	Strike Slip	4
Kocaeli	1999	7.51	Strike Slip	4
Chi-Chi Taiwan	1999	7.62	Reverse Oblique	36
Chi-Chi Taiwan-04	1999	6.2	Strike Slip	1
Chi-Chi Taiwan-06	1999	6.3	Reverse	2
Duzce Turkey	1999	7.14	Strike Slip	1
Denali Alaska	2002	7.9	Strike Slip	1
			Total	**202**

6.1 | Dimensionless intensity measures

A critical task for the probabilistic assessment of rocking structures under real seismic ground motions is the selection of adequate intensity measures (IMs) that correlate strongly with the structural demands. Previous studies have shown that rocking response is particulary sensitive to the velocity and acceleration characteristics of the ground motion, and have proposed IMs built upon the peak ground velocity PGV (e.g. $pPGV/g\tan\alpha$) and the peak ground acceleration PGA (e.g. $PGA/g\tan\alpha$)[20,22]. Petrone *et al.*[48] showed that velocity based IMs are more effective for large rocking structures ($R > 2$), whereas acceleration based IMs show a better correlation with smaller structures ($R < 1$). Likewise, several researchers[10,49,24] have stressed the importance of the duration and temporal signature of the ground-motion on rocking demands. For these reasons, in what follows, we have employed the dimensionless-orientationless IM, $p\,t_{uni}$, when assessing rocking demands (maximum rotation and angular acceleration of the safe rocking cases), whereas we have used $pPGV/g\tan\alpha$ when evaluating overturning fragilities.

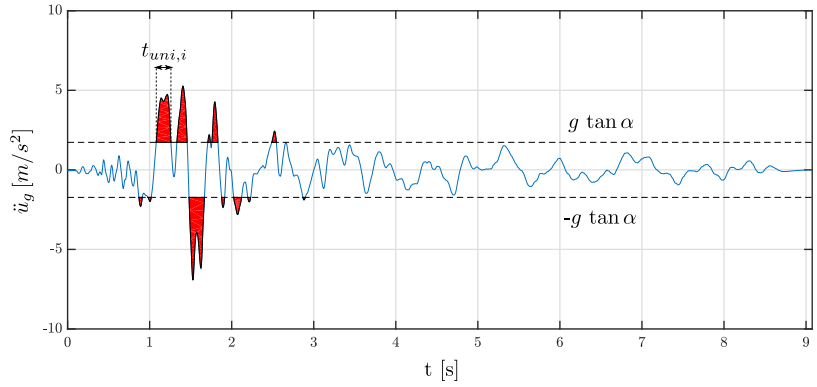

FIGURE 14 Dimentionless-orientationless IM for the rocking demands assessment: Uniform duration t_{uni}.

6.2 | Seismic demand analysis

We conducted a series of cloud analyses considering the earthquakes database described in Table 1 in order to assess the seismic demands of inerter-protected rocking structures. A stable slender block ($\alpha = 10°$, $R = 2[m]$ and $\eta = 0.85$) representative of a bridge pier or rocking column, was selected as a case of study in order to minimize the number of overturning events. Similarly to Section 5, the structural demands are described in terms of the dimensionless peak rotation, θ_{max}/α, and the dimensionless peak angular acceleration, $\ddot{\theta}_{max}/p^2\,\alpha$. A common assumption in seismic demand models is to consider that the median estimated demand, $\overline{D}_m$, follows a power law IM distribution:

$$\overline{D}_m = a\,IM^b \tag{24}$$

When plotted on a $ln(\overline{D}_m) - ln(IM)$ plane, Equation 24 becomes a straight line:

$$ln(\overline{D}_m) = ln(a) + b\,ln(IM) \tag{25}$$

where a and b are the linear regression coefficients. Figure 15 shows the results of the cloud analysis and the corresponding fitted seismic demand models for three cases: i) no inerter, ii) single inerter ($\sigma = 0.5$), and iii) pair of clutched-inerters ($\sigma = 0.5$).

The results of the regression analyses of Figure 15 show a strong correlation between the selected intensity measure, $p\,t_{uni}$, and the seismic demands, validating the estimation model proposed in Equation 24. Overall, the structures equipped with inerter devices show significantly smaller seismic demands for the whole range of IMs considered. In terms of maximum rotations (Figure 15a), reductions of around 30% are observed in the single inerter case, whereas the incorporation of the clutch further mitigates the seismic demands, reaching average reductions of around 55%. On the other hand, a reversed trend can be identified for the maximum angular accelerations. 25% lower demands are observed for the single inerter configuration, however, these values rise again when the clutch is introduced. This behaviour is consistent with the results obtained from the single pulse analyses presented in Section 5.

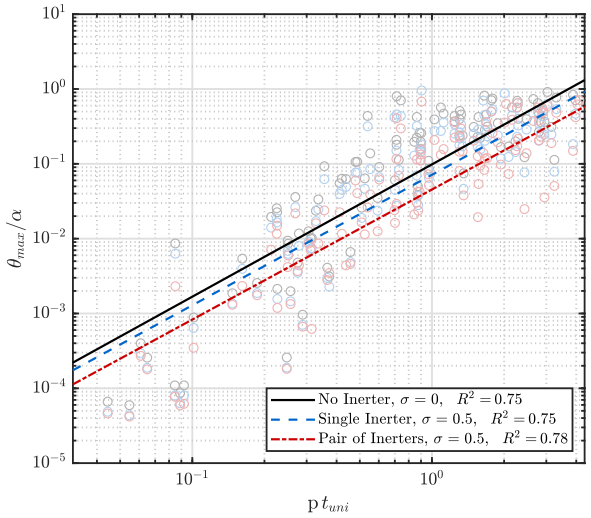

(a) Linear regression for the dimensionless peak rotation.

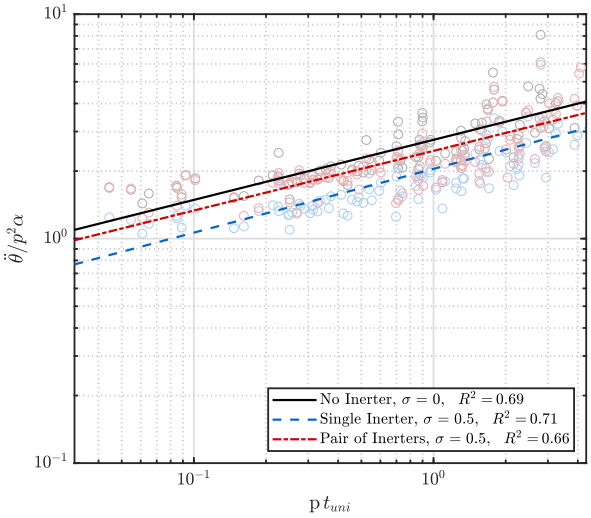

(b) Linear regression for the dimensionless peak angular acc.

FIGURE 15 Seismic demand analysis of a slender rigid block ($\alpha = 10°$, $R = 2[m]$ and $\eta = 0.85$) subjected to the suite of records described in Table 1.

6.3 | Probability of overturning

The probability of rocking overturning can be expressed as a categorical variable z_j, where $z = 1$ represents overturning, and $z = 0$ indicates safe or no rocking motion. Although the categorical nature of the response prevents the calculation of the statistical moments (mean μ and standard deviation β)[50], the overturning probability can be estimated following the maximum likelihood estimation (MLE)[51] approach assuming a log-normal distribution[22]. The MLE calculates the fragility function parameters, $\hat{\mu}$ and $\hat{\beta}$, that maximize the likelihood of reproducing the observed data, such that:

$$\{\hat{\mu}, \hat{\beta}\} = \max_{\mu,\beta} \prod_{j=1}^{n} \Phi\left(\frac{\ln x_j - \mu}{\beta}\right)^{z_j} \left(1 - \Phi\left(\frac{\ln x_j - \mu}{\beta}\right)\right)^{1-z_j} \tag{26}$$

where Φ is the normal cumulative distribution function and x_j the intensity measure values.

A small slender rigid block ($\alpha = 10°$, $R = 1[m]$ and $\eta = 0.85$), which is comparatively more unstable than the one considered above for assessing the seismic demands, was selected as a case study. Cloud analyses were then performed by considering the same suite of pulse-like ground motion records described in Table 1. Figure 16 plots the probability of overturning (P_{ro}) functions obtained for the three block configurations under study (no inerter, single inerter and pair of clutched-inerters) for apparent mass ratios of $\sigma = 0.5$ and 1.0. The graph also summarizes the data obtained from the numerical analyses. The y-coordinate of each circle represents the percentage of overturning observed for the corresponding IM strip, while the size scale of the circle indicates the number of observations.

The fragility functions depicted in Figure 16 show a significant improvement in the overturning performance of the block equipped with inerters. The estimated mean IM for the unprotected block is $\hat{\mu} = 1.08$, whereas this parameter increases to $\hat{\mu} = 1.22$ and $\hat{\mu} = 1.34$ when a single inerter and a pair of clutched-inerters with $\sigma = 0.5$ are employed. The overturning probabilities are further reduced if higher inertances are employed (i.e. $\sigma = 1.0$ in Figure 16b) where reductions in mean probabilities of toppling of over 50% are experienced for the clutched inerters configuration. These reduction levels are maintained for probabilities of exceedance of 10% as appreciated from Figure 16. These results are in line with the demand reductions observed in the previous section, and allows us to conclude that the use of a clutch is an efficient mechanism to reduce maximum rotations and improve the overturning response of rocking blocks under pulse-like ground motions. Nevertheless, the presence of the inerter almost duplicates the estimated standard deviation for $\sigma = 1.0$, leading to increased variability in the overturning estimation.

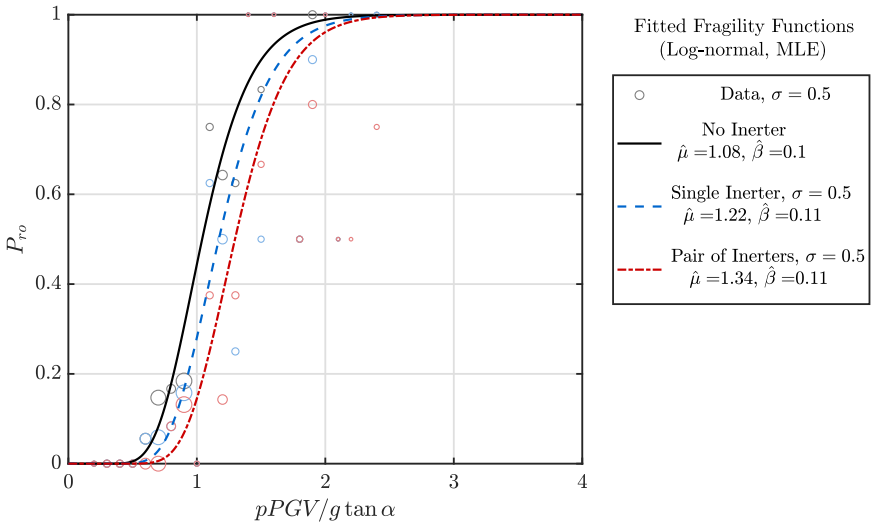

(a) Comparison of overturning probabilities for unprotected and protected cases with $\sigma = 0.5$.

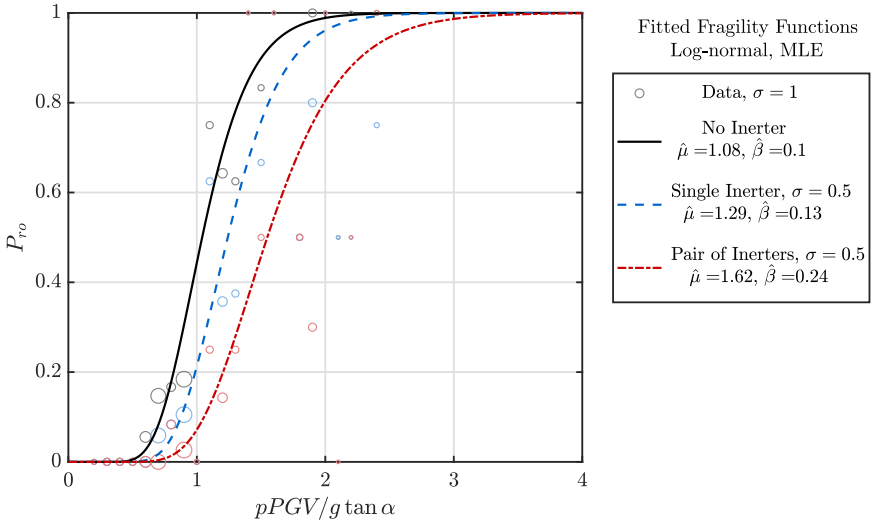

(b) Comparison of overturning probabilities for unprotected and protected cases with $\sigma = 1.0$.

FIGURE 16 Overturning fragility curves for a slender rigid block ($\alpha = 10°$, $R = 1[m]$ and $\eta = 0.85$) for different inertances σ.

7 | CONCLUSIONS

This paper explores the potential advantages of using supplemental rotational inertia to control the seismic response of rocking structures. The newly proposed system employs inerters, a mechanical device that develops a resisting force proportional to the relative acceleration between its terminals. These devices can be combined with a clutch to ensure they only oppose, and not lead, the rocking motion. We show that the inclusion of the inerter reduces the frequency parameter of the block resulting in lower seismic demands due to the well-known size effect of rocking behaviour. This finding is particularly interesting as it opens the possibility of modifying the dynamic characteristics of a rigid rocking block without altering its geometry.

Based on formal dimensional-orientational assessments of rocking block-inerter systems under single pulse excitations, we demonstrate that the rocking response of slender blocks with inerters remains perfectly self-similar if the mass ratio, σ, is incorporated as an additional dimentionless-orientationless parameter. On the other hand, the practical self-similarity in the response of non-slender blocks connected to a single inerter is preserved if the block slenderness, α, is eliminated as in independent group but this formulation becomes less accurate if a clutch is introduced, especially at later stages of the rocking response.

After examining the overturning of rocking structures under single pulse excitations through overturning plots, we find that the inclusion of the inerter reduces the overturning areas in the frequency-amplitude acceleration space and shifts them towards lower frequency regions. This frequency shift is particularly relevant for the cases of overturning after impact, as certain unprotected blocks that would survive the ground motion, may overturn when an inerter is attached. Besides, the added non-linearities brought about by the clutch result in inconsistent trends in the rocking response to sinusoidal pulses.

Rocking demands are also studied in terms of maximum rotations and peak angular accelerations. Overall, blocks equipped with a single inerter show smaller rotations and accelerations than unprotected ones. The incorporation of the clutch further reduces the rotation demands but at the expense of diminishing the acceleration reduction effects.

Finally, we conduct a probabilistic assessment of the seismic performance of protected and unprotected blocks using a set of 202 real pulse-like acceleration records. The results of this assessment confirm the behavioural trends observed under single pulse excitations. Firstly, blocks connected to a single inerter present lower maximum rotations and accelerations, while blocks with a pair of clutched-inerters experience some detrimental effects on their acceleration demands. Lastly, a comparison of the overturning fragility curves reveals that the inerter reduces the probability of overturning of the block, while the addition of the clutch further improves its resistance to overturning.

ACKNOWLEDGMENTS

The authors acknowledge the financial support of CONICYT (Consejo Nacional de Ciencia y Tecnología, Chile); Grant No 72170284

References

1. Konstantinidis D, Makris N. Seismic response analysis of multidrum classical columns. *Earthq Eng Struct Dyn.* 2005;34(10):1243–1270.

2. Psycharis IN, Lemos JV, Papastamatiou DY, Zambas C, Papantonopoulos C. Numerical study of the seismic behaviour of a part of the Parthenon Pronaos. *Earthq Eng Struct Dyn.* 2003;32(13):2063–2084.

3. Giouvanidis AI, Dimitrakopoulos EG. Seismic performance of rocking frames with flag-shaped hysteretic behavior. *JEngMech.* 2017;143(5):1–13.

4. Cheng CT. Shaking table tests of a self-centering designed bridge substructure. *Eng Struct.* 2008;30(12):3426–3433.

5. Kibriya LT, Málaga-Chuquitaype C, Kashani MM, Alexander NA. Nonlinear dynamics of self-centring rocking steel frames using finite element models. *Soil Dynamics and Earthquake Engineering.* 2018;115:826-837.

6. Solberg K., Mashiko N., Mander J. B., Dhakal R. P.. Performance of a damage-protected highway bridge pier subjected to bidirectional earthquake attack. *Journal of Structural Engineering.* 2009;135(5):469-478. Cited By :20.

7. Dowden D. M., Purba R., Bruneau M.. Behavior of self-centering steel plate shear walls and design considerations. *Journal of Structural Engineering (United States).* 2012;138(1):11-21. Cited By :26.

8. Dar A, Konstantinidis D, El-Dakhakhni WW. Evaluation of ASCE 43-05 seismic design criteria for rocking objects in nuclear facilities. *JStruct Eng.* 2016;:1–13.

9. Contento A, DiEgidio A. Investigations into the benefits of base isolation for non-symmetric rigid blocks. *Earthq Eng Struct Dyn.* 2009;38(7):849–866.

10. Housner GW. The Behavior of Inverted Pendulum Structures During Earthquakes. *Bulletin of the Seismological Society of America.* 1963;53:403-417.

11. Dimitrakopoulos EG, Giouvanidis AI. Seismic response analysis of the planar rocking frame. *JEngMech.* 2015;141(7):3426–3433.

12. Makris N, Vassiliou MF. Dynamics of the rocking frame with vertical restrainers. *JStructEng.* 2015;141(10):1–13.

13. Vassiliou MF, Burger S, Egger M, Bachmann JA, Broccardo M, Stojadinovic B. The three-dimensional behavior of inverted pendulum cylindrical structures during earthquakes. *Earthq Eng Struct Dyn.* 2017;46(14):2261–2280.

14. Vassiliou MF. Seismic response of a wobbling 3D frame. *Earthq Eng Struct Dyn.* 2017;47(5):1212–1228.

15. R R Truniger, Vassiliou MF, Stojadinovic B. An analytical model of a deformable cantilever structure rocking on a rigid surface: experimental validation. *Earthq Eng Struct Dyn.* 2015;44(15):2795–2815.

16. Makris N, Konstantinidis D. The rocking spectrum and the limitations of practical design methodologies. *Earthq Eng Struct Dyn.* 2003;32(2):265–289.

17. Chatzis MN, Espinosa MG, Smyth AW. Examining the energy loss in the inverted pendulum model for rocking bodies. *JEngMech.* 2017;:143:4017013.

18. Giouvanidis AI, Dimitrakopoulos EG. Nonsmooth dynamic analysis of sticking impacts in rocking structures. *Bull Earthquake Eng.* 2017;15(5):2273–2304.

19. Bachmann JA, Strand M, Vassiliou MF, Broccardo M, Stojadinovic B. Is Rocking Motion Predictable?. *Earthquake Engineering and Structural Dynamics.* 2018;47:535–552.

20. Ishiyama Y. Motions of rigid bodies and criteria for overturning by earthquake excitations. *Earthquake Eng Struct Dyn.* 1982;10(5):635–650.

21. Dimitrakopoulos EG, DeJong MJ. Revisiting the rocking block: closed-form solutions and similarity laws. *Proceedings of the Royal Society A: Mathematical, Physical and Engineering Sciences.* 2012;468:2294-2318.

22. Dimitrakopoulos EG, Paraskeva TS. Dimensionless fragility curves for rocking response to near-fault excitations. *Earthquake Eng Struct Dyn.* 2015;44(12):2015–2033.

23. Pappas A, Sextos A, DaPorto F, Modena C. Efficiency of alternative intensity measures for the seismic assessment of monolithic free-standing columns. *Bull Earthquake Eng.* 2017;15(4):1635–1659.

24. Dimitrakopoulos EG, Giouvanidis AI. Rocking amplification and strong-motion duration. *Earthquake Engng Struct Dyn.* 2018;:1–22.

25. Calio I, Marletta M. Passive control of the seismic rocking response of art objects. *Eng. Struct.* 2003;25(8):1009–1018.

26. Ceravolo R, Pecorelli ML, Fragonara L Zanotti. Semi-active control of the rocking motion of monolithic art objects. *J. Sound Vib.* 2016;374:1–16.

27. Makris N, Zhang J. Rocking response and overturning of anchored equipment under eeismic excitation. *PaciiňĄc Earthquake Engineering ResearchCentre, Berkeley.* 1999;.

28. Makris N, Zhang J. Rocking response of anchored blocks under pulse-type motions. *J. Eng. Mech.* 2001;127:484–493.

29. deLeo AM, Simoneschi G, Fabrizio C, DiEgidio A. On the use of a pendulum as mass damper to control the rocking motion of a rigid block with fixed characteristics. *Meccanica.* 2016;51(11):2727–2740.

30. Ceravolo R, Pecorelli ML, Fragonara LZ. Comparison of semi-active control strategies for rocking objects under pulse and harmonic excitations. *Mechanical Systems and Signal Processing.* 2017;90:175–188.

31. Vassiliou MF, Makris N. Analysis of the rocking response of rigid blocks standing free on a seismically isolated base. *Earthq Eng Struct Dyn.* 2012;41:177–196.

32. Arakaki T, Kuroda H, Arima F, Inoue Y, Baba K. Development of seismic devices applied to ball screw. Part 1: Basic performance of test RD-series. *AIJ J.Technol. Des.* 1999;8:239–244.

33. Ikago K, Saito K, Inoue N. Seismic control of single-degree-of-freedom structure using tuned viscous damper. *Earthquake Engineering and Structural Dynamics.* 2012;41(3):436–474.

34. Smith MC. Synthesis of mechanical networks: the inerter. *IEEE Trans. Autom. Control.* 2002;47(10):1648–1662.

35. Hwang JS, Kim J, Kim YM. Rotational Inertia Dampers with Toggle Bracing for Vibration Control of a Building Structure. *Engineering Structures.* 2007;29:1201–1208.

36. Makris N, Kampas G. Seismic protection of atructures with supplemental rotational inertia. *Journal of Engineering Mechanics.* 2016;142(11):1–11.

37. Lazar IF, Neild SA, Wagg DJ. Using an inerter-based device for structural vibration suppression. *Earthq Eng Struct Dyn.* 2014;43(8):1129–1147.

38. Giaralis A, Taflanidis AA. Reliability-based design of tuned mass-dampers-inerter (TMDI) equipped multi-storey frame buildings under seismic excitation. *Proc., 12th Int. Conf. on Applications of Statistics and Probability in Civil Engineering (ICASP12), T. Haukaas, ed., Vancouver, BC, Canada.* 2015;.

39. Clough RW, Penzien J. *Dynamics of structures*. McGraw-Hill, New York; 1975.

40. Chopra A. *Dynamics of structures: Theory and applications to earthquake engineering*. International Series in Civil Engineering and Engineering Mechanics, Prentice Hall, Upper Saddle River, NJ; 2000.

41. Makris N, Kampas G. Size versus slenderness: Two competing parameters in the seismic stability of free-standing rocking columns. *Bull. Seism. Soc. Am.* 2016;106(1):104–122.

42. Makris N, Vassiliou MF. Planar rocking response and stability analysis of an array of free-standing columns capped with a freely supported rigid beam. *Earthquake Eng Struct Dyn.* 2012;42(3):431–449.

43. ElGawady MA, Ma Q, Butterworth JW, Ingham J. Effects of interface material on the performance of free rocking blocks. *Earthq Eng Struct Dyn.* 2010;40:375âĂŞ392.

44. Makris N, Black CJ. Uplifting and overturning of equipment anchored to a base foundation. *Earthquakes Spectra.* 2002;18(4):631-661.

45. Vaschy A. Sur les lois de similitude en physique. *Annales Telegraphiques.* 1892;19:25–28.

46. Buckingham E. Model experiments and the forms of empirical equations. *Transactions American Society Mechanical Engineers.* 1915;37:263-296.

47. Anooshehpoor A, Heaton TH, Shi B, Brune JN. Estimates of the ground accelerations at point Reyes station during the 1906 San Francisco earthquake. *Bull. Seismol. Soc. Am.* 1999;89:845–853.

48. Petrone C, DiSarno L, Magliulo G, Cosenza E. Numerical modelling and fragility assessment of typical freestanding building contents. *Bull Earthquake Eng.* 2017;15(4):1609–1633.

49. Gelagoti F, Kourkoulis R, Anastasopoulos I, Gazetas G. Rocking-isolated frame structures: margins of safety against toppling collapse and simplified design approach. *Soil Dyn Earthquake Eng.* 2012;32(1):87–102.

50. Málaga-Chuquitaype C, Bougatsas K. Vector-IM-based assessment of alternative framing systems under bi-directional ground-motion. *Engineering Structures.* 2017;132:188–204.

51. Baker JW. Efficient analytical fragility function fitting using dynamic structural analysis. *Earthquake Earthq Spectra.* 2015;31(1):579–599.

How to cite this article: Thiers-Moggia R., Málaga-Chuquitaype C., (2018), Seismic protection of rocking structures with inerters, *Earthquake Engineering and Structural Dynamics*, DOI:10.1002/eqe.3147